International Journal of Mass Spectrometry xxx (2014) xxx–xxx

Contents lists available at ScienceDirect

International Journal of Mass Spectrometry

journal homepage: www.elsevier.com/locate/ijms

Combining tandem mass spectrometry with ion mobility separation to determine the architecture of polydisperse proteins

Dale A. Shepherd [a], Michael T. Marty [a], Kevin Giles [b], Andrew J. Baldwin [a], Justin L.P. Benesch [a,*]

[a] Department of Chemistry, Physical and Theoretical Chemistry Laboratory, University of Oxford, South Parks Road, Oxford OX1 3QZ, UK
[b] Waters Corporation, Stamford Avenue, Altrincham Road, Wilmslow SK9 4AX, UK

ARTICLE INFO

Article history:
Received 1 August 2014
Received in revised form 9 September 2014
Accepted 10 September 2014
Available online xxx

Keywords:
Collision-induced dissociation
Ion mobility spectrometry
Heterogeneity
Polydisperse protein
Time-aligned fragmentation
Post-ion mobility dissociation
Small heat-shock protein

ABSTRACT

Polydispersity presents a considerable challenge for the detailed molecular characterisation of many proteins. This is because in most biophysical and structural biology approaches the molecules in solution are ensemble-averaged, obscuring differences between individual proteins or conformational states. Mass spectrometry is however inherently dispersive, allowing the specific interrogation of molecules with distinct mass-to-charge ratios. Here, we exploit this intrinsic benefit to develop a means for determining directly the stoichiometries and sizes of oligomers comprising a polydisperse protein ensemble. Our method exploits the quadrupole-(ion-mobility)-(time-of-flight) geometry by submitting selected mass-to-charge ranges for ion mobility separation followed by collision-induced dissociation. In this sequential experiment the ion mobility information of the precursors is reported by the arrival times of the fragments, which are highly separated in mass-to-charge by virtue of the dissociation process. We observe small differences in the measured arrival time between fragments arising due to ion transit conditions after the ion mobility cell. To accommodate these systematic deviations, we develop a mass-to-charge dependent correction, leading to a reduction in the error of the collision cross-section measurement to around 0.5%. We characterise our method using HSP16.9, a small heat-shock protein that undergoes a mono- to polydisperse transition upon lowering pH, and reveal that the oligomers it forms have collisional cross-sections consistent with the polyhedral and double-ring architectures exhibited by other members of the protein family.

1. Introduction

Overcoming the inherent heterogeneity of biological macromolecules is one of the greatest challenges faced by modern structural molecular biology. This is because most techniques generally only provide data averaged over all molecules in solution and are therefore best suited to the study of highly homogeneous samples. Mass spectrometry (MS) has evolved into a technique capable of transferring proteins and the assemblies they form into the gas phase, while maintaining the majority of intra- and inter-molecular non-covalent interactions [1–8]. As a result, it has the ability to provide a snapshot of the equilibrium distribution of molecules in solution by isolating them from each other in vacuum, and analysing them according to their mass-to-charge (m/z) ratio. In this way MS allows the components that comprise a heterogeneous biomolecular ensemble to be interrogated individually within the mass spectrometer [9].

Ion mobility spectrometry (IM) has emerged as a useful approach for structural biology, complementing MS data to provide insights into the quaternary structure, dynamics, and assembly processes of proteins [7,9–12]. By capitalising on the separation afforded in m/z, IM–MS has proven to be particularly useful in the analysis of species present in heterogeneous samples, providing low-resolution structural information in terms of collisional cross-sections (CCSs) on the multiple states populated at equilibrium. Nonetheless, when different states overlap in both m/z and IM arrival time, it is not currently possible to unambiguously obtain accurate masses and CCSs. However, this difficulty can in principle be circumvented either by increasing the IM resolving power, or the separation between populated charge states. The

* Corresponding author. Tel.: +44 1865 285420.
E-mail address: justin.benesch@chem.ox.ac.uk (J.L.P. Benesch).

http://dx.doi.org/10.1016/j.ijms.2014.09.007
1387-3806/

most practical means of achieving this is the latter: by implementing charge reduction, leading to larger m/z ratios, and thereby greater separation between adjacent charge states.

Charge reduction can be conducted in a number of ways including through the use of solution additives [13,14], ion–ion [15–18], and ion-neutral chemistries [19–21]. However, the most popular approach used in the study of protein complexes exploits the mechanism of collision-induced dissociation (CID), which tends to remove ≈50% of the charge on the complexes and has the helpful corollary of reducing the number of bound adducts that otherwise lead to line-broadening in the mass spectra [22]. When subjected to CID, protein complexes usually dissociate via the unfolding and loss of one or more monomeric subunits [23]. During this unfolding process, charge migration occurs in order to reduce coulombic repulsion over the protein complex surface. This results in the unfolded monomer carrying a disproportionate amount of the original charge in relation to its mass [24–28]. Because charge is conserved in this process, the residual "stripped" complex has a much lower charge than the precursor.

In general, for the case of a homo-oligomer of n subunits, the singly stripped complex produced during CID will have $(n-1)$ subunits and appear at higher m/z than the intact oligomer. At higher energies, further dissociation events can occur in a sequential manner, giving rise to stripped complexes of $(n-2)$, $(n-3)$, ... subunits [29]. In these cases, the loss of multiple subunits means each successive stripped complex will appear at progressively higher m/z ratios with ever greater separation between adjacent charge states [30,31]. Because monomer loss is the predominant dissociation pathway for protein assemblies, measuring the masses of the dissociated monomer and the stripped complex provides a straightforward method to back-calculate the mass of the precursor ion.

We, and others, have demonstrated that a CID-based approach is a very useful means for obtaining stoichiometry information for several polydisperse protein ensembles for which the MS spectra are rendered uninterpretable due to extensive peak overlap. Through removing highly charged monomers by means of CID, we achieved sufficient charge-state separation to determine the oligomeric distributions of an archetypal polydisperse protein, the human small heat-shock protein (sHSP) αB-crystallin [30,32–34]. We also combined this approach with IM–MS experiments, performed in parallel, to investigate the three-dimensional structure of the same protein [35]. However, due to the overlap of charge states in the IM–MS data, we could only obtain arrival times for a selected sub-population of oligomers within the mixture and therefore had to impose a number of assumptions to fit our data and estimate arrival times for the individual oligomeric states [35].

To improve on the ambiguity of this method, one logical approach is to perform IM and CID experiments on the same ions in sequence such that CCSs may be determined directly. However, it is critical to maintain protein complex structure throughout the IM device in order to obtain accurate CCS values, as any activation will inevitably lead to changes in complex structure and eventually unfolding and dissociation [23]. Such distortions will necessarily be reported by the IM measurement if collisional activation is carried out beforehand, and the observed CCS will therefore not be representative of the solution structure of the protein under investigation. However, performing CID after IM will yield arrival time data that are not compromised in this way because the ions are already mobility-separated prior to their activation. In this case, product ions with distinct m/z ratios from the precursor will appear at the same arrival time in the IM data, a phenomenon sometimes referred to as "time-alignment" [36,37]. In other words, it would be possible to infer the arrival time of the precursor ion directly from the products.

Here, we develop a post-IM CID approach to deconvolute the charge states of polydisperse proteins and thereby determine both the stoichiometries and CCSs of the constituent oligomeric states. To test our approach, we examine HSP16.9 from wheat, a 201 kDa member of the sHSP family that has been shown to exhibit a highly dynamic quaternary structure [38]. We find that, upon lowering pH, HSP16.9 switches from a monodisperse dodecamer to populate a polydisperse ensemble, making it an ideal system to test our methodology. We first apply the MS–IM–CID–MS approach to monodisperse HSP16.9 to assess the fidelity of IM data when ions are subject to high post-IM accelerating voltages. We observe minor but reproducible changes in the arrival-time distributions (ATDs) upon acceleration that we attribute to a combination of phenomena occurring during CID and ion transfer to the time-of-flight analyser (ToF), and introduce an acceleration-dependent arrival time correction to correct for them.

We apply our method to polydisperse HSP16.9 to obtain arrival times for >80 peaks from the product ions observed in time-aligned IM-CID spectra. We find that the CCS of HSP16.9 increases approximately linearly with the number of subunits over the range of 4- to 24-mers. By using a combination of coarse-grained and atomistic structural modelling, and validation with electron microscopy data, we show that HSP16.9 adopts globular topologies, consistent with the polyhedral and double-ring architectures observed for other members of the sHSPs. In conclusion, we suggest that the MS–IM–CID–MS method we present here will prove useful in the structural interrogation of a wide range of polydisperse and heterogeneous biomolecular systems.

2. Materials and methods

2.1. Protein preparation

HSP16.9 was expressed and purified as described previously [39]. Each aliquot of protein solution was buffer-exchanged into 200 mM ammonium acetate (pH 5 or 6.9) using MicroBioSpin-6 spin columns (BioRad) and incubated at laboratory temperature for at least 30 min before analysis.

2.2. IM–MS experiments

Nanolectrospray (nESI) IM–MS experiments were carried out on a travelling-wave Q-IM-ToF mass spectrometer (Synapt G2 HDMS, Waters Corp., Wilmslow, UK), according to previously described protocols [40], and with instrument settings optimised for the transmission of intact noncovalent protein complexes [41]. Experiments were conducted in positive polarity and ion mobility mode with the following instrument settings, unless otherwise stated: capillary voltage 1.4 kV, sample cone 20 V, extraction cone 1 V, trap acceleration voltage 4 V, trapping time 500 μs, trap/transfer gas flow (argon) 10 ml min^{-1} (pressure 0.044 mbar), helium cell flow rate 120 ml min^{-1}, IM wave height 30 V, IM wave velocity 700 ms^{-1}, IM gas flow 50 ml min^{-1} (pressure 4.2 mbar), transfer wave height 1 V, transfer wave velocity 65 ms^{-1}. For post-IM CID experiments dissociation was achieved by increasing the transfer acceleration voltage in the range 60–160 V. The value of the enhanced duty cycle delay coefficient [42,43] used for our experiments was 1.57 ms $Th^{-1/2}$.

CCS values were obtained from the experimental arrival-time data using established methods [43,44], employing as calibrants the native protein complexes avidin, alcohol dehydrogenase and glutamate dehydrogenase, which give good coverage of the mobility range analysed [45]. All data were initially analysed using Masslynx software (Waters Corp., Wilmslow, UK), and the distribution of oligomeric states populated by HSP16.9 was

Please cite this article in press as: D.A. Shepherd, et al., Combining tandem mass spectrometry with ion mobility separation to determine the architecture of polydisperse proteins, Int. J. Mass Spectrom. (2014), http://dx.doi.org/10.1016/j.ijms.2014.09.007

estimated using a probability-based deconvolution algorithm operating on the MS dimension of the data [46].

2.3. Structure modelling

Three different coarse-grained structural models were constructed, and their trend in CCS as a function of mass was fitted by least squares minimisation to the average experimental CCS over all charge states for each oligomeric state, accounting for the range and 0.5% error in CCS after drift time correction. (1) For the "spherical model" of mass m the trend $CCS = am^{2/3}$ was fitted to the data with a being a free parameter collecting together factors including the mass density. (2) For the "dimer stack model", dimensions of a single dimer were approximated as a cuboid of $19 \times 30 \times 60$ Å through comparison with the core domain dimer from the structure of the dodecamer (PDB ID: 1GME) [39], and multiples thereof used as minimum constraints for even numbered complexes when fitting to the experimental data. (3) For the "hollow sphere model" the trend was based on an increase in radius of the central cavity, r_{cavity}, according to $r_{cavity} = am^b$, with a and b as free parameters. The outer radius was taken as $r_{outer} = r_{cavity} + d$, where d is the minimum thickness of a dimeric protomer (19 Å, from PDB ID: 1GME) [39], and $CCS = \pi r_{outer}^2$ was fitted to the experimental CCS data.

Pseudo-atomic models were built as described previously [35], using the dimeric core domain excised from the HSP16.9 crystal structure (Residues 44-136, PDB ID: 1GME) [39]. Briefly, a database of different architectural scaffolds, containing convex polyhedra and ring-like architectures, was constructed. For model construction, the dimeric building-block of HSP16.9 was placed on the edge of each architecture and the inter-dimer distance adjusted such that they were 2 Å apart. The PDB file output was used for CCS calculation using the CCS Calc projection approximation algorithm (Waters Corp., Wilmslow, UK), and a linear scaling factor of 1.14 applied to the theoretical values to allow comparison with experimental measurements [9].

2.4. Negative-stain transmission electron microscopy

HSP16.9 (pH 5) was diluted to 50 nM and immobilised on carbon-coated copper 300 mesh grids (Electron Microscopy Sciences, Hatfield, PA, USA), and stained with uranyl acetate solution (2% w/v). Grids were visualised on a JEOL 2010 transmission electron microscope operating at 200 kV and equipped with a $2K \times 2K$ CCD camera. Images were processed using the Xmipp electron microscopy image analysis software [47], with 200 particles manually selected in 256×256 pixel boxes and sorted into 10 classes.

3. Results and discussion

3.1. Asymmetric partitioning of charge during CID improves separation between adjacent charge-states

HSP16.9 is a well-characterised member of the sHSP family that exists as a monodisperse dodecamer (12 subunits) at neutral pH [39]. We obtained an IM–MS spectrum of HSP16.9 under gentle ionisation and ion transfer conditions in order to preserve the three-dimensional structure of the protein complex (Fig. 1A). The spectrum exhibits a single charge-state distribution, centred on the 32+ charge state and corresponding to a mass of 200,940 Da. This agrees well with a dodecamer carrying a small number of low molecular weight adducts, and the m/z projection of the data (Fig. 1A, upper panel) matches closely our previous MS results [38,48]. Examination of the IM dimension reveals that each charge state has a narrow and approximately Gaussian ATD, suggesting a single conformational family, and after calibration reveals a measured CCS of 8760 Å [2]. This compares favourably to that

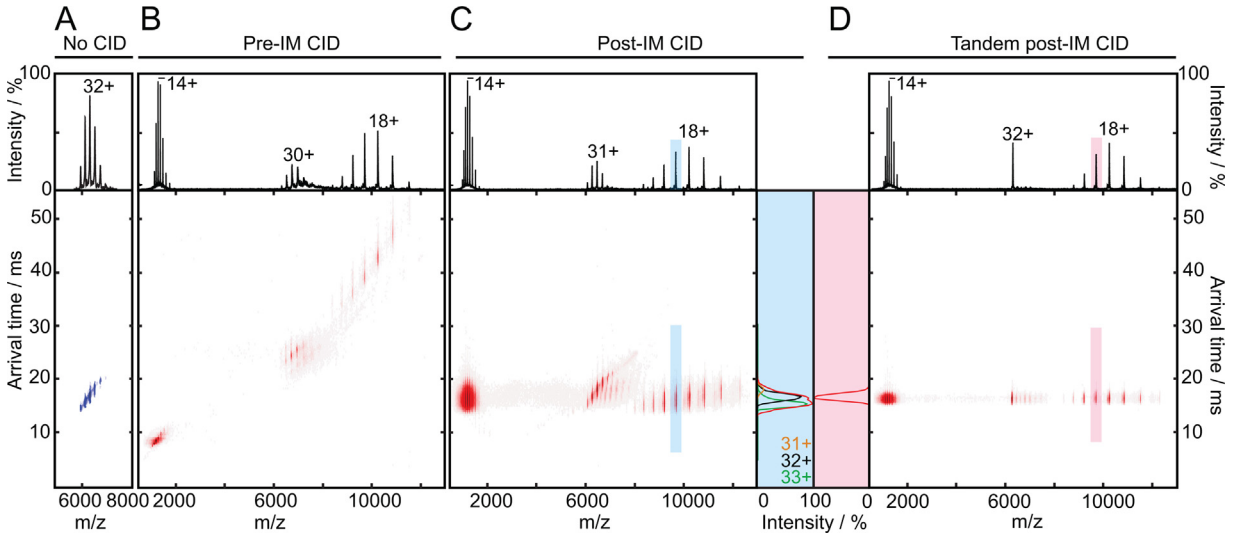

Fig. 1. Post-IM CID yields time-aligned ATDs for CCS determination. (A) HSP16.9 is a dodecamer at pH 6.9, exhibiting a single, narrow charge state distribution centred on 32+ (upper panel). Under non-activating conditions the IM spectrum displays a single Gaussian ATD for each charge state (lower panel), consistent with retention of native protein structure. (B) Pre-IM CID results in asymmetric charge partitioning between an unfolded monomeric subunit at low m/z and a charge-reduced undecamer at high m/z (upper panel). Because CID is carried out pre-IM, ion activation and dissociation are evident in the IM-MS spectrum (lower panel), with intact precursor ions displaying a shift to longer arrival times and product ions separating as a function of CCS/z. Information on the native-like protein conformation is therefore lost in this experiment. (C) Post-IM CID also results in the appearance of monomers and undecamers (upper panel), yet in this case they are time-aligned to the dodecamer (lower panel). However, the product ions possess ATDs that are a convolution of several precursor charge states (blue box). (D) Mass selection using the quadrupole analyser prior to IM and CID (i.e. MS–IM–CID–MS) yields time-aligned product ions that possess ATDs stemming from only a single precursor charge state (pink box), allowing the unambiguous determination of CCS. (For interpretation of the references to colour in this figure legend, the reader is referred to the web version of this article.)

Please cite this article in press as: D.A. Shepherd, et al., Combining tandem mass spectrometry with ion mobility separation to determine the architecture of polydisperse proteins, Int. J. Mass Spectrom. (2014), http://dx.doi.org/10.1016/j.ijms.2014.09.007

expected from the crystal structure (8702 Å [2]), suggesting that HSP16.9 is present in a form closely resembling that in solution, with the absence of significant compaction or unfolding in the vacuum of the mass spectrometer.

In our instrument, it is possible to effect collisional activation after the quadrupole in two collision cells, one situated before the IM cell and the other after ("trap" and "transfer", respectively). To examine the effects of conducting CID pre-IM, we accelerated HSP16.9 into the trap with a potential of 90 V (Fig. 1B). Signal is observed at low m/z corresponding to monomers (mass 16,724 Da, centred on the 14+ charge state), and at high m/z corresponding to undecamers (11 subunits, 184,090 Da, 18+) (Fig. 1B, upper panel). Notably, the spacing between adjacent charge states is significantly increased for the undecamers relative to the dodecamers. This is a direct consequence of the monomer having carried away an amount of charge disproportionate to its mass, leaving a singly stripped complex of much lower charge than the parent. The CID products are also separated in the IM dimension, with monomers appearing at ≈10 ms, and the undecamers over the range 35–50 ms. Concomitant to this dissociation, the parent dodecamers have shifted to higher arrival times (≈25 ms), relative to minimally activating conditions (≈18 ms, Fig. 1A). This is consistent with unfolding of the dodecamers prior to monomer ejection. Clearly, performing CID prior to IM, though effective for charge reduction, results in complete loss of information on the native structure.

3.2. MS–IM–CID–MS results in time-alignment of precursor and product ions

As an alternative strategy, we performed CID after IM separation by accelerating HSP16.9 ions into the transfer collision cell (Fig. 1C). We observed that the dodecamer ions dissociate into monomer and undecamer product ions. In order to obtain suitably intense signal for the dissociation products at high m/z we found it crucial to optimise the instrument settings, specifically the pressure in the transfer (trap/transfer gas flow rate: 10 ml min^{-1}), and both the transfer wave height (1 V) and wave velocity (65 ms^{-1}). In particular, a transfer wave height above 15 V resulted in a significant drop-off in signal intensity. The appearances of the mass spectra obtained in this post-IM CID experiment are essentially indistinguishable from those obtained by performing CID pre-IM (compare upper panels of Fig. 1B,C). Notably, however, in the IM dimension the spectra are very different. Whereas for pre-IM CID the product ions are distributed over a wide arrival time range (Fig. 1B), for post-IM CID the product ions all appear at ≈18 ms, as was the case for the dodecamers prior to activation (Fig. 1A). The product ions are thus time-aligned with the precursors.

These experiments clearly demonstrate the possibility of inferring the arrival times of the precursors from the arrival times of the products. However, in order to determine CCSs of the ions in question it is necessary to know the charge state and mass of the precursor from which the products arise. In this case, where HSP16.9 populates only dodecamers, and the spectrum is simple, obtaining the mass of the precursor is straightforward. However, multiple precursor charge states can contribute to a particular product charge state (e.g. 31+, 32+ and 33+ dodecamers all give rise to the 18+ undecamer signal) (Fig. 1C, blue box). As a result, the product ions' ATDs are a superposition of contributions, and cannot be readily used to determine the CCS of the precursor.

To address this challenge, we can perform a prior stage of MS, such that we submit only a particular precursor charge state to dissociation. Using the quadrupole of the instrument, we selected the 32+ charge state of the HSP16.9 dodecamer and performed post-IM CID. Analogous to our previous spectrum, this yielded a

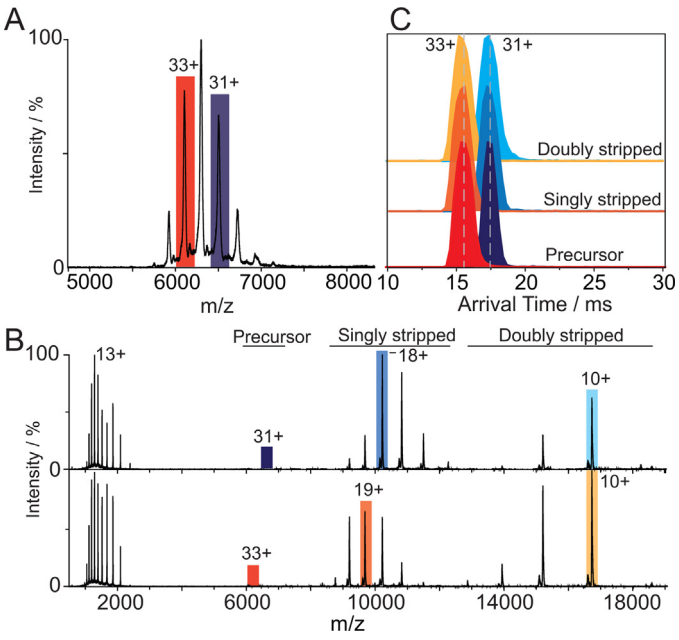

Fig. 2. Precursor arrival time information is maintained over multiple post-IM dissociation steps. (A) The 31+ and 33+ charge states of monodisperse HSP16.9 dodecamers were isolated for CID. (B) Post-IM CID yields monomers and both undecamers and decamers, i.e. singly ($n-1$) and doubly stripped ($n-2$) complexes. (C) The ATDs of the dodecamers (33+, navy; 31+ red) are well separated in arrival time. This separation is maintained upon dissociation of the precursors into both singly (blue; orange) and doubly stripped (light blue; light orange) ions at elevated transfer collision voltages. Close examination reveals however that there are minor changes in the appearance of the ATDs over the two dissociation steps. (For interpretation of the references to colour in this figure legend, the reader is referred to the web version of this article.)

spectrum with monomer and undecamer product ions that are time-aligned with the precursor (Fig. 1D). Having selected only a particular precursor of known charge state for dissociation, we have all the information required to reconstruct its CCS from the time-aligned product ions.

3.3. Acceleration of ions after IM leads to minor but systematic changes in arrival time

To assess whether the CID conditions have any influence on the ATDs obtained, we selected individually the 31+ and 33+ charge states of the dodecamer and subjected them to increasing accelerating voltages into the transfer cell (Fig. 2A). In both cases, monomers and undecamers were observed above 70 V (Fig. 2B as in Fig. 1D). At higher voltages (above 120 V), new peaks appeared at >14000 m/z, corresponding to decamers formed by further dissociation of the undecamers (Fig. 2B) [29]. Having originated through the loss of two highly charged monomers, adjacent charge states of these doubly stripped ions are very well separated. We extracted the ATDs for the decamer and undecamer to compare with those obtained for the dodecamer (Fig. 2C). For both 31+ and 33+ charge states, the ATDs obtained from both singly ($n-1$) and doubly stripped ($n-2$) complexes did not differ greatly from that of the precursor. However, close inspection of the ATDs uncovers very slight differences in peak shape and centroid value. This reveals that although CCS information is preserved over two CID steps, a small error is introduced as a result, arising either as a direct result of the applied acceleration voltage, or indirectly through the dissociation it causes.

To examine these systematic changes in ATD occurring during post-IM activation, we interrogated the IM–MS standards avidin,

Please cite this article in press as: D.A. Shepherd, et al., Combining tandem mass spectrometry with ion mobility separation to determine the architecture of polydisperse proteins, Int. J. Mass Spectrom. (2014), http://dx.doi.org/10.1016/j.ijms.2014.09.007

alcohol dehydrogenase (ADH) and glutamate dehydrogenase (GDH). Both ADH and GDH are resistant to CID below an acceleration potential of 200 V, allowing the ATDs of the intact oligomers to be examined over a wide voltage range. Taking ADH as an example, a clear shift towards shorter arrival times is observed with increasing acceleration into the transfer, an effect that is not significantly attenuated upon increasing the wave height (Fig. 3A). For ADH, a decrease of up to 0.4 ms (≈2.2% at a ToF pusher interval of 274 μs) is observed for the oligomer, with the largest shift attained at ≈70 V, after which the arrival time plateaus (Fig. 3A,B). We performed similar experiments on avidin and GDH and observed a small but reproducible shift in all cases to shorter arrival times caused by acceleration into the transfer.

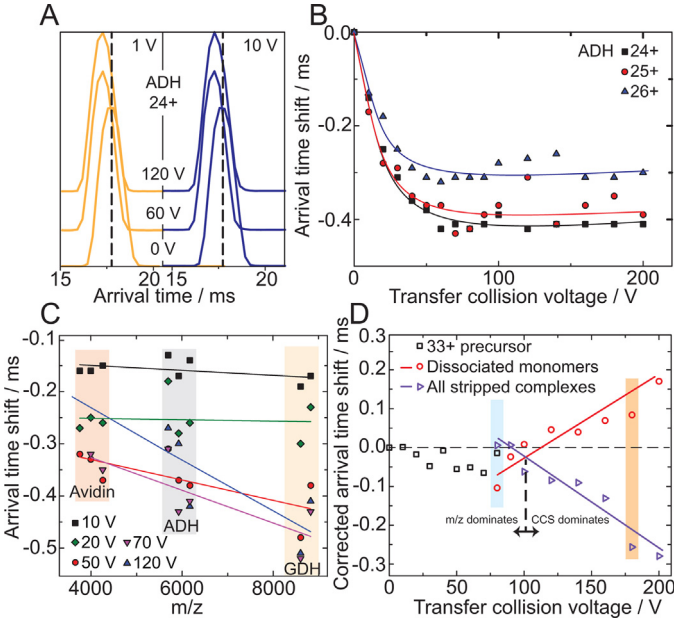

Fig. 3. Small changes in arrival time caused by high accelerating energies can be accommodated. (A) Experimental ATDs of the ADH tetramer 24+ charge state show a small but reproducible shift to shorter arrival times as acceleration into the transfer is increased between 0 and 60 V. There is little change in the shift at higher collision voltages, shown here for 120 V, and it is essentially identical at transfer travelling-wave heights of 1 V (left, orange) and 10 V (right, blue). (B) This shift in ATD is observed for all charge states, with the arrival time of ADH initially decreasing to a minimum at around 70 V, and reaching a plateau at higher voltages. This can be explained by the increased velocity of ions leading to shorter ion transfer times after IM separation, to a minimum naturally limited by the time spent in the drift cell. (C) Plots of this arrival time shift versus m/z for each of the standards avidin, ADH and GDH at a range of transfer acceleration voltages reveal a strong m/z dependence at higher voltage. This m/z- and voltage dependence can be applied as a correction to the experimental arrival time data of unknowns in order to minimise the error in CCS associated with the arrival time shift. (D) Imposing this correction to data obtained for the 33+ charge state of HSP16.9 dodecamer minimises the spread in arrival time to around 0.1 ms (black squares). At a transfer voltage of 80 V (blue box), the threshold for dissociation, the monomers (red circles) and stripped oligomers (violet triangles) of HSP16.9 appear at distinct arrival times to the dodecamer. We rationalise this separation by the differences in m/z between products and precursor, which results in variations in the flight-time between the transfer and the ToF pusher. As the voltage is increased, monomers get progressively retarded, whereas the stripped oligomers transit faster. This reversal in arrival time can be explained by considering the CCS-dependent collisions the ions undergo with the bath gas in the transfer ion guide that act to slow the ions down. The monomer arrival time therefore increases as a function of voltage due to progressive unfolding, whereas that of the stripped complex decreases, consistent with collapse. These hypothesised changes in arrival time as a result of disruption of ion structure are validated by pre-IM CID experiments (Fig. S1B). (For interpretation of the references to colour in this figure legend, the reader is referred to the web version of this article.)

3.4. Accelerated ions traverse the transfer cell faster than the travelling waves

To understand the origin of the decrease in arrival time, we considered the instrument geometry and resulting contributions to the arrival time (t_A) measurement. t_A comprises both the IM drift time (t_D) and the time spent between the IM cell and the ToF pusher (t_0). The flight time of ions in the ToF is not considered, as the arrival-time-stamp is recorded as the start of each individual push, as opposed to when the ions impinge on the detector. In our instrument, t_0 is composed of an m/z dependent term ($t_{m/z}$) that describes the transit time between the exit of the transfer cell and entrance of the ToF pusher, and the time spent in the transfer cell (t_{Trans}) which is generally assumed to be governed by the travelling-wave velocities and hence be m/z independent. Therefore $t_A = t_D + t_{m/z} + t_{Trans}$, with changes in $t_{m/z}$ or t_{Trans} both potentially contributing to variations in arrival time observed in the data. In the absence of dissociation, $t_{m/z}$ may be considered as a constant, as the m/z values of the ions are essentially invariant as a function of accelerating voltage. Therefore, in the first instance, we can limit our initial discussion to t_{Trans}.

We anticipate that, as ions are accelerated to high kinetic energies by the transfer voltage, they can travel faster through the transfer cell than dictated by the travelling wave, leading to a decrease in t_{Trans}. To consider this in more detail, we note that in our instrument the transfer cell is 131 mm long and comprises 87 plate electrodes: one DC followed by 43 pairs over which the travelling-wave potentials operate. Therefore, for the transfer wave velocity of 65 m s^{-1} used in our experiments, an upper limit for t_{Trans} can be estimated at 2.01 ms, ≈13% of the arrival time of the 33 + HSP16.9 dodecamer ion at these instrument settings. The transfer collision voltage is applied between plates 25 and 26, 36.5 mm into the device (n.b. different generations of Synapt instrumentation implement the collision voltage differently). As a result, the ions only feel the effects of acceleration over the last 94.5 mm of the cell (a residence time of 1.45 ms at 65 m s^{-1}). The maximum decrease in arrival time for the precursor ions we observe is considerably smaller (0.4 ms, Fig. 3B). This means that the decrease in t_A can be explained entirely by a decrease in t_{Trans} brought about by ions exceeding the wave velocity after acceleration by the transfer voltage (i.e. 'skipping' over waves) prior to their thermalisation through collisions with the bath gas[1]. This also provides a rationale for the fact that the transfer travelling wave height does not significantly alter the observed arrival time shifts (Fig. 3A), as the accelerating potential is considerably higher than the potential barrier provided by the highest wave height at which we obtain sufficient ion current.

3.5. Acceleration-dependent arrival time correction

These observations for the IM protein standards allow us to develop a framework to account for this effect in the analysis of unknowns. In principle, it is possible to carry out separate

[1] Using simple collision theory, in which the collision cross-section of the ion is assumed constant, it is possible to approximate the deceleration of the ions as they progress through the transfer cell [49]. We can compare this to the wave height and wave velocity, and thereby gauge the number of waves overhauled. However, due to difficulties in determining the exact pressure and gas composition in the transfer we can only put an upper limit on this number. For ADH^{24+}, at 60 V acceleration, wave height 1 V, and under our experimental conditions (see Section 2), we obtain an estimate of 5 waves. At the wave velocity of 65 ms^{-1} this corresponds to a decrease in arrival time of 0.9 ms. While this number is likely only accurate within a small factor, being higher than that observed (0.4 ms) is consistent with the unfolding of the ADH ions upon activation, leading to an increase in CCS.

Please cite this article in press as: D.A. Shepherd, et al., Combining tandem mass spectrometry with ion mobility separation to determine the architecture of polydisperse proteins, Int. J. Mass Spectrom. (2014), http://dx.doi.org/10.1016/j.ijms.2014.09.007

calibrations over each of the acceleration voltages, however, a less laborious alternative is to use a calibration at a single (low) reference acceleration voltage, and incorporate an m/z- and voltage-dependent correction. Specifically, we apply the observed m/z dependent arrival-time shift observed for the calibrant ions of avidin, ADH and GDH at each transfer voltage studied (with high m/z ions exhibiting a greater shift at high voltage than at low voltage, Fig. 3C). Considering the HSP16.9 dodecamer ions as a function of transfer voltage, a shift in arrival time is observed with increasing acceleration voltage, with the largest decrease of 0.45 ms at ≈70 V (Fig. S1A), similar to our observations for the standards (Fig. 3B). Applying the acceleration voltage correction acts to correct the absolute shift relative to the precursor, confining the overall spread of arrival times of the precursor to within ±0.1 ms (<0.6%, which corresponds to <0.2% in CCS).

At 80 V, the threshold for CID is reached, and both monomers and undecamers appear in the spectrum. Interestingly, even after correction, the monomers appear about ≈0.1 ms earlier than the dodecamers, and the stripped complexes slightly later (Fig. 3D, blue). Remarkably, as the voltage is increased further, the monomers become progressively retarded, such that they arrive ≈0.5 ms later than the stripped oligomers at 200 V (Fig. 3D, orange). Nonetheless, even at the highest voltage, the arrival time of each product reproduces that of the precursor ±0.25 ms (<1.4% in arrival time, which corresponds to ≈0.5% in CCS, reduced from around 1.4% in CCS prior to correction). This demonstrates that, provided care is taken to accommodate the effect of transfer acceleration voltage, post-IM CID can be used for the determination of accurate CCS values for protein complexes by the analysis of time-aligned product ions.

3.6. A combination of m/z and CCS dependent effects cause variations in the arrival times of product ions

To explain the surprising arrival time phenomena observed for HSP16.9 above the threshold voltage for CID, we considered the properties of the instrument geometry and our understanding of protein assemblies upon collisional activation. At 80 V transfer acceleration, the arrival time of the monomers is shorter than the dodecamer, which is in turn shorter than that of the undecamer: $t_A^{1mer} < t_A^{12mer} < t_A^{11mer}$. However, since t_D is invariant for all three ions, these differences are a result of changes in $t_{m/z}$ or t_{Trans}. This can be considered by noting that the m/z ratios follow the rank order $m/z^{1mer} < m/z^{12mer} < m/z^{11mer}$ (see Fig. 1B). In the region between the transfer and pusher the ions will become separated by m/z-dependent time-of-flight. Estimation of $t_{m/z}$ for the monomer (14+), dodecamer (33+) and undecamer (18+) yields values of 0.05, 0.12 and 0.16 ms, respectively (see Section 2). The differences in $t_{m/z}$ estimated for these three ions match well with the shifts observed experimentally at 80 V, suggesting that at the threshold for dissociation, m/z effects alone can account for the variations in arrival time (Fig. 3D).

At higher accelerating voltages (>100 V), the reverse order of arrival times is observed: $t_A^{1mer} > t_A^{12mer} > t_A^{11mer}$. As m/z is

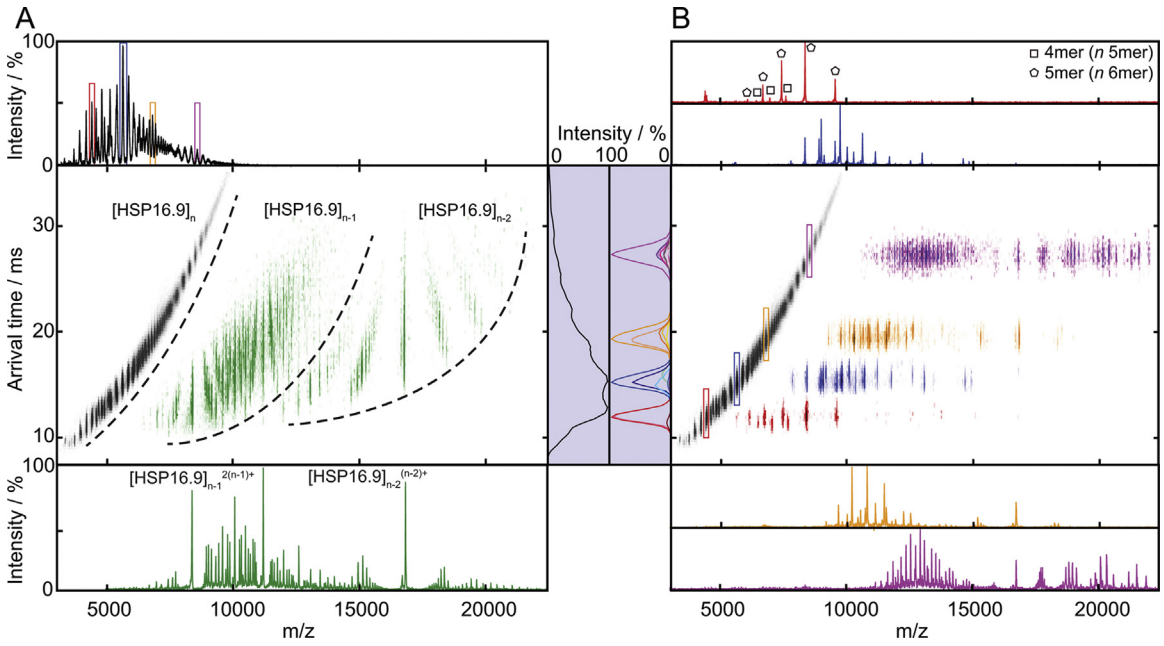

Fig. 4. MS–IM–CID–MS allows ATDs to be extracted for the complexes comprising an heterogeneous ensemble. (A) HSP16.9 exhibits a complex mass spectrum at pH 5, characteristic of polydispersity (top panel). Signals overlap in both the m/z and arrival time dimensions, rendering ATDs of the individual oligomers unatainable by usual methods (middle panel, black). Upon activation in the transfer collision cell, HSP16.9 oligomers of n subunits undergo dissociation by loss of one and two monomers to yield charge-reduced oligomers with $(n-1)$ and $(n-2)$ subunits, respectively (middle and lower panels, green). These singly and doubly stripped oligomers separate into distinct regions of the IM–MS spectrum due to the conservation of charge between dissociation products (middle panel, green; boundaries indicated by dashed, curved lines). While stoichiometries can be assigned from these data, the arrival time dimension remains a superposition of many overlapping species (violet box, black trace). (B) In order to obtain ATDs for individual stoichiometries we perform mass selection (middle panel, and (A), coloured boxes) using the quadrupole analyser and subject the precursors to CID to yield time-aligned spectra for precursors of a defined m/z (colours match those in (A)). From these spectra, the stoichiometries of the precursor can be readily assigned through knowledge of whether the product contains either $(n-1)$ or $(n-2)$ subunits, and arrival times extracted for each stoichiometry (violet box, coloured traces). For example, the spectrum in red shows the CID spectrum obtained after selection at 4400 m/z, and yields tetramers (squares) and pentamers (pentagons) in the $(n-1)$ region of the spectrum, which in the IM dimension report on the arrival times of pentamers and hexamers, respectively. In this way ATDs for oligomers ranging from 4- to 24-mers were obtained. Knowledge of the mass and m/z window that was selected for CID can be used to determine the charge state of the precursor. This in turn enables conversion of arrival time to CCS after calibration and the application of our m/z- and voltage-dependent arrival time correction (Fig. 3). (For interpretation of the references to colour in this figure legend, the reader is referred to the web version of this article.)

Please cite this article in press as: D.A. Shepherd, et al., Combining tandem mass spectrometry with ion mobility separation to determine the architecture of polydisperse proteins, Int. J. Mass Spectrom. (2014), http://dx.doi.org/10.1016/j.ijms.2014.09.007

essentially invariant with accelerating voltage, these changes in t_A must stem from differences in t_{Trans}. One possible cause is variations in CCS with increasing activation. Within the transfer cell the pressure is sufficiently high (measured at 0.044 mbar, but inevitably higher in the vicinity of the exit aperture of the IM cell) that ions will undergo collisions, retarding them in a CCS-dependent manner [49]. The observed effect is consistent with the monomers increasing in size (due to unfolding) with increasing activation and the stripped complexes decreasing (due to collapse). To test this hypothesis, we performed pre-IM CID of HSP16.9 and examined the arrival times of the products as a function of trap acceleration voltage (Fig. S1B). In this experiment, we find that monomers increase in arrival time and undecamers decrease. This is consistent with similar data obtained for another dodecameric sHSPs undergoing pre-IM CID [23]. Physically, this behaviour can be explained by considering both the rate and extent of structural distortion brought about by collisional activation. At higher accelerating voltages, the internal energy required for a given structural distortion is reached more quickly, i.e. earlier in the collision cell [50]. As a result, the ions will spend a longer time in their distorted state, giving them more time to undergo separation by CCS and to progress down the collapse/unfolding pathway. The behaviour of the HSP16.9 monomer and stripped complex ions, relative to the dodecameric precursor, can therefore be explained by invoking a combination of m/z and CCS dependent effects.

3.7. Tandem post-IM CID enables deconvolution of complex IM–MS data

Having characterised the MS–IM–CID–MS approach, we investigated its utility in the study of a polydisperse protein assembly. HSP16.9 is generally described as monodisperse dodecamer at neutral pH and ambient solution temperatures [38,39,48], giving rise to a single charge-state distribution in the mass spectra (Fig. 1A). However, native IM–MS of the same protein at pH 5 reveals a broad region of signal spanning 3500–10,000 m/z and 8–35 ms (Fig. 4A, black). The spectrum is similar to that observed for other polydisperse protein complexes and arises from the overlap of many charge states from multiple co-populated stoichiometries (Fig. 4A, top) [35]. As a result, neither the IM nor MS dimensions of the data can be readily interpreted in terms of the individual oligomeric states.

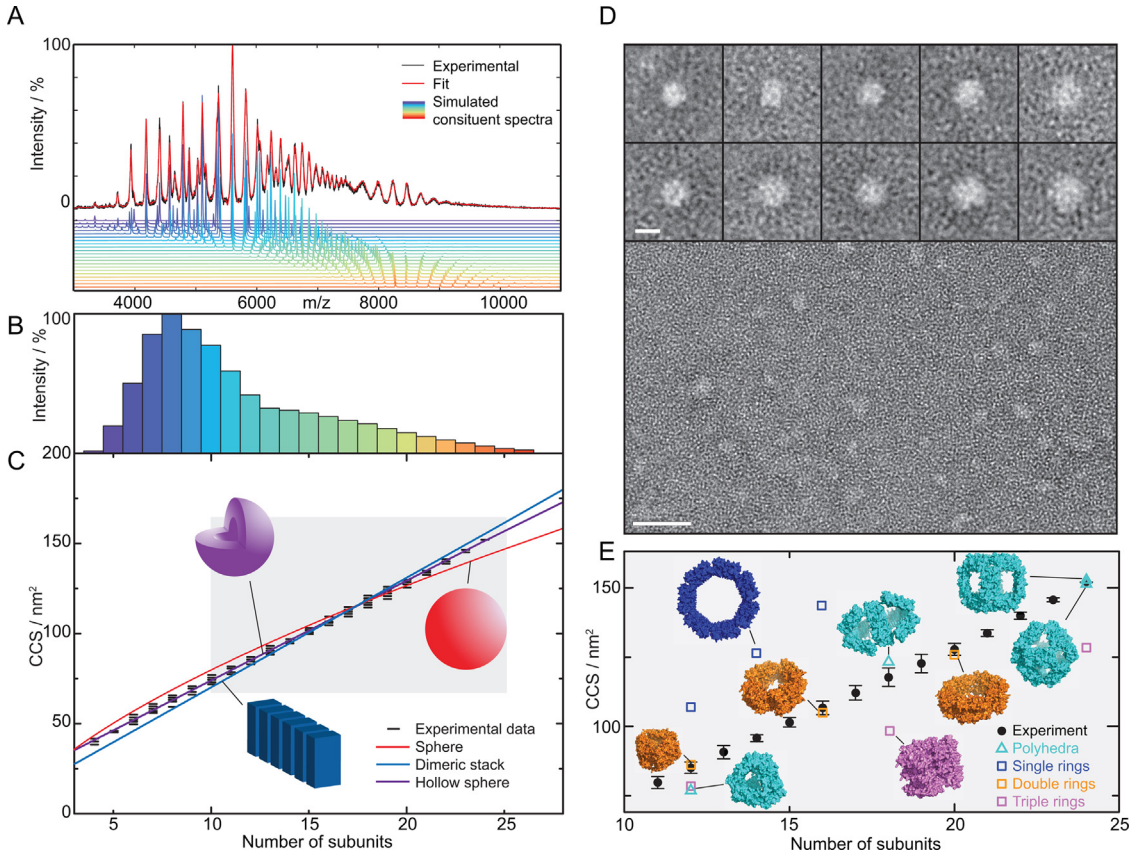

Fig. 5. The oligomers formed by HSP16.9 are consistent with polyhedral and double-ring architectures. (A) Estimating the oligomeric distribution of HSP16.9 at pH 5 using a probability-based mass spectrum deconvolution approach reveals a very close fit between the experimental data (black) and sum (red) of multiple oligomeric states (each line corresponding to one oligomeric state, ranging from small to large (violet to red, respectively). (B) This deconvolution suggests the presence of oligomers spanning from tetramers to 26-mers (top panel), which fits well with the oligomeric states positively identified in the tandem-MS data (Fig. 4). (C) A plot of CCS obtained using our MS–IM–CID–MS strategy reveals a linear trend with number of subunits (black, one dash for each charge state). The experimental trends do not agree with coarse-grained models built on a stack of dimers (blue line) or a sphere of constant density (red). However the data is reproduced well by a model based on a spherical shell (purple line). (D) Negative stain TEM data obtained for HSP16.9 at pH 5 reveals a range of particle sizes (lower panel, scale bar = 50 nm). Classification of 200 particles yields class averages that are consistent with globular complexes (upper panel, scale bar = 10 nm), validating the IM–MS data. (E) Comparison of pseudo-atomic models (coloured, selected structures shown) built using ring-like and polyhedral scaffolds compared to the experimental data (black), enables us to rule out single- (blue) and triple-ring (violet) arrangements. However, our data fit well the CCSs determined for double-ring (orange) and polyhedral (cyan) models, consistent with HSP16.9 forming globular complexes with a central cavity and with the known structures of other members of the sHSP family. (For interpretation of the references to colour in this figure legend, the reader is referred to the web version of this article.)

Please cite this article in press as: D.A. Shepherd, et al., Combining tandem mass spectrometry with ion mobility separation to determine the architecture of polydisperse proteins, Int. J. Mass Spectrom. (2014), http://dx.doi.org/10.1016/j.ijms.2014.09.007

Accelerating all HSP16.9 ions into the transfer cell (i.e. IM–CID–MS, without selection in the quadrupole) yields a spectrum with a large number of features spread over a wide m/z range (Fig. 4A, green) resulting from the charge–reduction that occurs during CID. The m/z dimension is very well resolved, with certain peaks being particularly intense due to the overlap of multiple oligomeric states, a phenomenon characteristic of mass spectra of polydisperse proteins [30,51] (Fig. 4A, lower panel). As a consequence of the conservation of charge during CID, the singly and doubly stripped product ions separate into distinct regions of IM–MS space. However, although the masses of the oligomers can now be measured from these data, their CCSs cannot be determined because the charge states of the precursor ions that give rise to specific product ions are unknown.

To overcome this ambiguity, we isolated 30 narrow m/z windows over the range 4000–9000 m/z using the quadrupole analyser, and submitted them individually to post-IM CID (Fig. 4C). For each selection, we assigned the product ions and identified their corresponding precursor ion based on whether they were singly or doubly stripped. For example, after selection at 4400 m/z and CID, the spectrum displays product-ion signals corresponding to HSP16.9 tetramers and pentamers (Fig. 4B, red). Because these appear in the region of the spectrum consistent with singly stripped $(n-1)$ product ions, we identify them as stemming from pentameric and hexameric precursors (n). Armed with this knowledge of their mass, we can readily determine their charge state through dividing by the m/z ratio at which the quadrupole selection was made.

In this way, from our 30 selections we could assign >80 different charge states at good signal-to-noise ratios, corresponding to all stoichiometries ranging from 4- to 24-mers, and extract their individual ATDs. To verify that this tandem-MS approach provided good coverage of the oligomers comprising the ensemble, we performed a deconvolution of the native mass spectrum (Fig. 5A), using a probability-based approach [46]. This suggested an oligomeric distribution spanning from 4 to 26 subunits (Fig. 5B), in excellent agreement with that measured experimentally. This demonstrates that our MS–IM–CID–MS approach provides an effective means for interrogating essentially the entire oligomeric distribution of the polydisperse ensemble. Notably, the distribution is centred on an octamer, and, unlike the mammalian sHSP αB-crystallin [52], shows no preference for oligomers containing an even number of subunits.

3.8. The CCSs of polydisperse HSP16.9 are consistent with established sHSP architectures

To obtain structural information on the different oligomeric states populated by HSP16.9 at pH 5, we converted the ATDs for all the identified peaks into CCSs, using the calibration and arrival-time correction detailed above. A plot of the CCS against number of subunits reveals a linear relationship, with little variation in CCS as a function of charge state for each stoichiometry (Fig. 5B). To evaluate the shape of the complexes, we assessed three extensible structural forms to see whether they are consistent with the data: a linear stack of dimeric building blocks ("dimer stack"); a sphere of constant density ("spherical"), and a hollow spherical shell ("hollow sphere"). For each model, the best trend of CCS versus mass was obtained by fitting to the experimental data (Fig. 5B). The spherical model dictates an inherently curved trend, which fits the data poorly, and, while the dimeric stack reproduces the linearity well, it underestimates the CCS for the lower stoichiometries and overestimates at the higher stoichiometries. The hollow sphere model, however, fits the data extremely well across the full range of observed stoichiometries. To cross-validate this conclusion, we obtained negative stain transmission electron microscopy (TEM) images of HSP16.9 at pH 5, selecting 200 particles for classification. All the resulting 10 class-averages displayed globular rather than linear features, in line with the IM–MS data (Fig. 5D).

To generate simple pseudo-atomic models consistent with both with a globular shape and our understanding of the structure of other members of the sHSP family [53,54], we considered ring-like and polyhedral architectures. The models were constructed as previously described [35], using the structure of the dimeric HSP16.9 core domain as the protomeric building block. Comparison of the experimental data with the CCSs calculated for the various models allows us to reject a number of them, and reveal a number of very close matches (Fig. 5E). We find that, across the oligomeric range, the single-ring models (blue) were too large to fit the data, whereas the triple-rings (violet) are too small. However, the structures based on double-ring (orange) and polyhedral (cyan) architectures match the data well. For some stoichiometries, multiple possible structures were in agreement with our data, e.g. both the octahedron and cube fit the CCS measured for the 24-mer. The possibility of HSP16.9 forming double-rings is consistent with the published crystal structure of the HSP16.9 dodecamer [39], and may represent an additional framework for self-assembly that complements the polyhedral arrangements we have observed previously for αB-crystallin [35].

4. Conclusions

We have described a new strategy for the study of polydisperse proteins by performing an MS–IM–CID–MS experiment. This approach capitalises on the efficient charge reduction resulting from CID to separate the overlapping signal in the native mass spectrum over a wide m/z range, such that oligomers can be interrogated individually. We have demonstrated that the mobility information in this experiment can be maintained across multiple dissociation steps, with the product ions time-aligned with the precursor. The small shift in arrival time caused by the high accelerating potentials applied to effect CID can be readily accommodated by applying a voltage-dependent correction to the data, minimizing the error in CCS.

We have exemplified the utility of our approach by investigating HSP16.9, a member of the sHSP family of chaperones that undergoes a surprising switch from monodisperse dodecamer to polydisperse ensemble at low pH. We obtained CCSs from more than 80 charge states stemming from HSP16.9 oligomers comprising between 4 and 24 subunits. The resulting trend of CCS with oligomeric state is consistent with a continuum of globular structures with a central cavity, and is in close agreement with pseudo-atomic models built on the polyhedral and double-ring architectures known for other sHSPs. In sum, our work demonstrates that CCSs may be determined for all the oligomers comprising a highly polydisperse protein, laying the groundwork for structural investigations of other heterogeneous biomolecules by means of IM–MS.

Acknowledgements

We thank Prof Eman Basha (Ta'if University) and Prof Elizabeth Vierling (University of Massachusetts, Amherst) for providing purified HSP16.9; Prof Dame Carol Robinson (University of Oxford) for support; Prof Kevin Pagel (Free University Berlin) for preliminary experiments and helpful discussions; Dr Neil Young and Dr Robert Jacobs (University of Oxford) for initial help with EM experiments; Dr Jonathan Hopper (University of Oxford) for critical assessment of the manuscript; and the Engineering and Physical Sciences Research Council grant EP/J01835X/1 for funding. AJB holds a David Phillips Fellowship from the Biotechnology and

Biosciences Research Council, and JLPB a Royal Society University Research Fellowship.

Appendix A. Supplementary data

Supplementary data associated with this article can be found, in the online version, at http://dx.doi.org/10.1016/j.ijms.2014.09.007.

References

[1] J. Snijder, A.J.R. Heck, Analytical approaches for size and mass analysis of large protein assemblies, Annu. Rev. Anal. Chem. (Palo Alto. Calif.) 7 (2014) 43–64.
[2] G.R. Hilton, J.L.P. Benesch, Two decades of studying non-covalent biomolecular assemblies by means of electrospray ionization mass spectrometry, J. R. Soc. Interface 9 (2012) 801–816.
[3] A. Konijnenberg, A. Butterer, F. Sobott, Native ion mobility-mass spectrometry and related methods in structural biology, Biochim. Biophys. Acta 1834 (2013) 1239–1256.
[4] S.J. Hyung, B.T. Ruotolo, Integrating mass spectrometry of intact protein complexes into structural proteomics, Proteomics 12 (2012) 1547–1564.
[5] K. Thalassinos, A.P. Pandurangan, M. Xu, F. Alber, M. Topf, Conformational States of macromolecular assemblies explored by integrative structure calculation, Structure 21 (2013) 1500–1588.
[6] J.T.S. Hopper, C.V. Robinson, Mass spectrometry quantifies protein interactions – from molecular chaperones to membrane porins, Angew. Chem. Int. Ed. Engl. (2014) , doi:http://dx.doi.org/10.1002/anie.201403741R1 (in press).
[7] F. Lanucara, S.W. Holman, C.J. Gray, C.E. Eyers, The power of ion mobility-mass spectrometry for structural characterization and the study of conformational dynamics, Nat. Chem. 6 (2014) 281–294.
[8] M. Sharon, Structural MS pulls its weight, Science 340 (2013) 1059–1060.
[9] J.L.P. Benesch, B.T. Ruotolo, Mass spectrometry: come of age for structural and dynamical biology, Curr. Opin. Struct. Biol. 21 (2011) 641–649.
[10] C. Uetrecht, R.J. Rose, E. van Duijn, K. Lorenzen, A.J.R. Heck, Ion mobility mass spectrometry of proteins and protein assemblies, Chem. Soc. Rev. 39 (2010) 1633–1655.
[11] R. Beveridge, Q. Chappuis, C. Macphee, P.E. Barran, Mass spectrometry methods for intrinsically disordered proteins, Analyst 138 (2013) 32–42.
[12] Y. Zhong, S.J. Hyung, B.T. Ruotolo, Ion mobility-mass spectrometry for structural proteomics, Inf. Healthc. 9 (2012) 47–58.
[13] K. Pagel, S. Hyung, B.T. Ruotolo, C.V. Robinson, Alternate dissociation pathways identified in charge-reduced protein complex ions, Anal. Chem. 82 (2010) 5363–5372.
[14] M.I. Catalina, R.H.H. van den Heuvel, E. van Duijn, A.J.R. Heck, Decharging of globular proteins and protein complexes in electrospray, Chem. A Eur. J. 11 (2005) 960–968.
[15] M. Scalf, M.S. Westphall, L.M. Smith, Charge reduction electrospray mass spectrometry, Anal. Chem. 72 (2000) 52–60.
[16] Q. Zhao, et al., An ion trap-ion mobility-time of flight mass spectrometer with three ion sources for ion/ion reactions, J. Am. Soc. Mass Spectrom. 20 (2009) 1549–1561.
[17] I.D.G. Campuzano, P.D. Schnier, Coupling electrospray corona discharge, charge reduction and ion mobility mass spectrometry: from peptides to large macromolecular protein complexes, Int. J. Ion Mobil. Spectrom. 16 (2013) 51–60.
[18] R.R. Abzalimov, I.A. Kaltashov, Electrospray ionization mass spectrometry of highly heterogeneous protein systems: protein ion charge state assignment via incomplete charge reduction, Anal. Chem. 82 (2010) 7523–7526.
[19] R.E. Bornschein, S. Hyung, B.T. Ruotolo, Ion mobility-mass spectrometry reveals conformational changes in charge reduced multiprotein complexes, J. Am. Soc. Mass Spectrom. 22 (2011) 1690–1698.
[20] D. Bagal, et al., Gas phase stabilization of noncovalent protein complexes formed by electrospray ionization, Anal. Chem. 81 (2009) 7801–7806.
[21] J.T.S. Hopper, K. Sokratous, N.J. Oldham, Charge state and adduct reduction in electrospray ionization-mass spectrometry using solvent vapor exposure, Anal. Biochem. 421 (2012) 788–790.
[22] J.L.P. Benesch, C.V. Robinson, Mass spectrometry of macromolecular assemblies: preservation and dissociation, Curr. Opin. Struct. Biol. 16 (2006) 245–251.
[23] J.L.P. Benesch, Collisional activation of protein complexes: picking up the pieces, J. Am. Soc. Mass Spectrom. 20 (2009) 341–348.
[24] S.N. Wanasundara, M. Thachuk, Toward an improved understanding of the dissociation mechanism of gas phase protein complexes, J. Phys. Chem. B 114 (2010) 11646–11653.
[25] I. Sinelnikov, E.N. Kitova, J.S. Klassen, Influence of coulombic repulsion on the dissociation pathways and energetics of multiprotein complexes in the gas phase, J. Am. Soc. Mass Spectrom. 18 (2007) 617–631.
[26] J.C. Jurchen, E.R. Williams, Origin of asymmetric charge partitioning in the dissociation of gas-phase protein homodimers, J. Am. Chem. Soc. 125 (2003) 2817–2826.
[27] B.T. Ruotolo, et al., Ion mobility-mass spectrometry reveals long-lived, unfolded intermediates in the dissociation of protein complexes, Angew. Chemie Int. Ed. 46 (2007) 8001–8004.
[28] S.V. Sciuto, J. Liu, L. Konermann, An electrostatic charge partitioning model for the dissociation of protein complexes in the gas phase, J. Am. Soc. Mass Spectrom. 22 (2011) 1679–1689.
[29] J.L.P. Benesch, J.A. Aquilina, B.T. Ruotolo, F. Sobott, C.V. Robinson, Tandem mass spectrometry reveals the quaternary organization of macromolecular assemblies, Chem. Biol. 13 (2006) 597–605.
[30] J.A. Aquilina, J.L.P. Benesch, O.A. Bateman, C. Slingsby, C.V. Robinson, Polydispersity of a mammalian chaperone: mass spectrometry reveals the population of oligomers in alphaB-crystallin, Proc. Natl. Acad. Sci. U. S. A. 100 (2003) 10611–10616.
[31] C. Uetrecht, et al., High-resolution mass spectrometry of viral assemblies: molecular composition and stability of dimorphic hepatitis B virus capsids, Proc. Natl. Acad. Sci. U. S. A. 105 (2008) 9216–9220.
[32] J.L.P. Benesch, M. Ayoub, C.V. Robinson, J.A. Aquilina, Small heat shock protein activity is regulated by variable oligomeric substructure, J. Biol. Chem. 283 (2008) 28513–28517.
[33] A.J. Baldwin, H. Lioe, C.V. Robinson, L.E. Kay, J.L.P. Benesch, αB-crystallin polydispersity is a consequence of unbiased quaternary dynamics, J. Mol. Biol. 413 (2011) 297–309.
[34] G.R. Hilton, et al., C-terminal interactions mediate the quaternary dynamics of αB-crystallin, Philos. Trans. R. Soc. Lond. B Biol. Sci. 368 (2013) 20110405.
[35] A.J. Baldwin, et al., The polydispersity of αB-crystallin is rationalized by an interconverting polyhedral architecture, Structure 19 (2011) 1855–1863.
[36] C.W.N. Damen, et al., Electrospray ionization quadrupole ion-mobility time-of-flight mass spectrometry as a tool to distinguish the lot-to-lot heterogeneity in *N*-glycosylation profile of the therapeutic monoclonal antibody trastuzumab, J. Am. Soc. Mass Spectrom. 20 (2009) 2021–2033.
[37] J. Castro-Perez, et al., Localization of fatty acyl and double bond positions in phosphatidylcholines using a dual stage CID fragmentation coupled with ion mobility mass spectrometry, J. Am. Soc. Mass Spectrom. 22 (2011) 1552–1567.
[38] F. Sobott, J.L.P. Benesch, E. Vierling, C.V. Robinson, Subunit exchange of multimeric protein complexes. Real-time monitoring of subunit exchange between small heat shock proteins by using electrospray mass spectrometry, J. Biol. Chem. 277 (2002) 38921–38929.
[39] R.L. Van Montfort, E. Basha, K.L. Friedrich, C. Slingsby, E. Vierling, Crystal structure and assembly of a eukaryotic small heat shock protein, Nat. Struct. Biol. 8 (2001) 1025–1030.
[40] H. Hernández, C.V. Robinson, Determining the stoichiometry and interactions of macromolecular assemblies from mass spectrometry, Nat. Protoc. 2 (2007) 715–726.
[41] Campuzano, I. D. G., Giles, K. in Methods Mol. Biol. 790 57–70 (2011).
[42] K. Giles, et al., Applications of a travelling wave-based radio-frequency-only stacked ring ion guide, Rapid Commun. Mass Spectrom. 18 (2004) 2401–2414.
[43] B.T. Ruotolo, J.L.P. Benesch, A.M. Sandercock, S. Hyung, C.V. Robinson, Ion mobility-mass spectrometry analysis of large protein complexes, Nat. Protoc. 3 (2008) 1139–1152.
[44] D.P. Smith, et al., Deciphering drift time measurements from travelling wave ion mobility spectrometry-mass spectrometry studies, Eur. J. Mass Spectrom. 15 (2009) 113–130.
[45] M.F. Bush, et al., Collision cross sections of proteins and their complexes: a calibration framework and database for gas-phase structural biology, Anal. Chem. 82 (2010) 9557–9565 (Supp Info).
[46] M.T. Marty, H. Zhang, W. Cui, M.L. Gross, S.G. Sligar, Interpretation and deconvolution of nanodisc native mass spectra, J. Am. Soc. Mass Spectrom. 25 (2014) 269–277.
[47] S.H.W. Scheres, R. Núñez-Ramírez, C.O.S. Sorzano, J.M. Carazo, R. Marabini, R, Image processing for electron microscopy single-particle analysis using XMIPP, Nat. Protoc. 3 (2008) 977–990.
[48] J.L.P. Benesch, F. Sobott, C.V. Robinson, Thermal dissociation of multimeric protein complexes by using nanoelectrospray mass spectrometry, Anal. Chem. 75 (2003) 2208–2214.
[49] A.C. Gill, K.R. Jennings, T. Wyttenbach, M.T. Bowers, Conformations of biopolymers in the gas phase: a new mass spectrometric method, Int. J. Mass Spectrom. 195–196 (2000) 685–697.
[50] J.L.P. Benesch, B.T. Ruotolo, D.A. Simmons, C.V. Robinson, Protein complexes in the gas phase: technology for structural genomics and proteomics, Chem. Rev. 107 (2007) 3544–3567.
[51] A.M. Smith, T.R. Jahn, A.E. Ashcroft, S.E. Radford, Direct observation of oligomeric species formed in the early stages of amyloid fibril formation using electrospray ionisation mass spectrometry, J. Mol. Biol. 364 (2006) 9–19.
[52] G.K.A. Hochberg, J.L.P. Benesch, Dynamical structure of αB-crystallin, Prog. Biophys. Mol. Biol. 115 (2014) .
[53] G.R. Hilton, H. Lioe, F. Stengel, A.J. Baldwin, J.L.P. Benesch, Small heat-shock proteins: paramedics of the cell, Top. Curr. Chem. 328 (2013) 69–98.
[54] E. Basha, H. O'Neill, E. Vierling, Small heat shock proteins and α-crystallins: dynamic proteins with flexible functions, Trends Biochem. Sci. 37 (2012) 106–117.

Please cite this article in press as: D.A. Shepherd, et al., Combining tandem mass spectrometry with ion mobility separation to determine the architecture of polydisperse proteins, Int. J. Mass Spectrom. (2014), http://dx.doi.org/10.1016/j.ijms.2014.09.007